



A regional CO₂ observing system simulation experiment for the ASCENDS satellite mission

J. S. Wang^{1,2}, S. R. Kawa², J. Eluszkiewicz^{3,†}, D. F. Baker⁴, M. Mountain³, J. Henderson³, T. Nehr Korn³, and T. S. Zaccheo³

¹Universities Space Research Association, Columbia, MD, USA

²NASA Goddard Space Flight Center, Greenbelt, MD, USA

³Atmospheric and Environmental Research, Lexington, MA, USA

⁴Cooperative Institute for Research in the Atmosphere, Colorado State University, Fort Collins, CO, USA

[†]deceased on 27 May 2014

Correspondence to: J. S. Wang (james.s.wang@nasa.gov)

Received: 19 February 2014 – Published in Atmos. Chem. Phys. Discuss.: 20 May 2014

Revised: 9 October 2014 – Accepted: 15 October 2014 – Published: 8 December 2014

Abstract. Top-down estimates of the spatiotemporal variations in emissions and uptake of CO₂ will benefit from the increasing measurement density brought by recent and future additions to the suite of in situ and remote CO₂ measurement platforms. In particular, the planned NASA Active Sensing of CO₂ Emissions over Nights, Days, and Seasons (ASCENDS) satellite mission will provide greater coverage in cloudy regions, at high latitudes, and at night than passive satellite systems, as well as high precision and accuracy. In a novel approach to quantifying the ability of satellite column measurements to constrain CO₂ fluxes, we use a portable library of footprints (surface influence functions) generated by the Stochastic Time-Inverted Lagrangian Transport (STILT) model in combination with the Weather Research and Forecasting (WRF) model in a regional Bayesian synthesis inversion. The regional Lagrangian particle dispersion model framework is well suited to make use of ASCENDS observations to constrain weekly fluxes in North America at a high resolution, in this case at 1° latitude × 1° longitude. We consider random measurement errors only, modeled as a function of the mission and instrument design specifications along with realistic atmospheric and surface conditions. We find that the ASCENDS observations could potentially reduce flux uncertainties substantially at biome and finer scales. At the grid scale and weekly resolution, the largest uncertainty reductions, on the order of 50 %, occur where and when there is good coverage by observations with low measurement errors and the a priori uncertainties are large.

Uncertainty reductions are smaller for a 1.57 μm candidate wavelength than for a 2.05 μm wavelength, and are smaller for the higher of the two measurement error levels that we consider (1.0 ppm vs. 0.5 ppm clear-sky error at Railroad Valley, Nevada). Uncertainty reductions at the annual biome scale range from ~ 40 % to ~ 75% across our four instrument design cases and from ~ 65% to ~ 85 % for the continent as a whole. Tests suggest that the quantitative results are moderately sensitive to assumptions regarding a priori uncertainties and boundary conditions. The a posteriori flux uncertainties we obtain, ranging from 0.01 to 0.06 Pg C yr⁻¹ across the biomes, would meet requirements for improved understanding of long-term carbon sinks suggested by a previous study.

1 Introduction

Quantification of surface fluxes of CO₂ and other greenhouse gases (GHG) over a range of spatial and temporal scales is of critical importance for understanding the processes that drive source/sink variability and climate–biogeochemistry feedbacks. The need to monitor GHG fluxes also follows from climate policy initiatives such as the Kyoto Protocol and possible follow-on agreements, along with their implementation (e.g., emissions trading and treaty verification). While direct “bottom-up” (inventory) approaches are considered accurate to within 10 % in the annual mean for fossil fuel CO₂ emissions in North America (Gurney et al., 2009), “top-

down” (inverse) methods are the tool of choice to infer CO₂ sources and sinks from the terrestrial biosphere and oceans on a range of scales (Peters et al., 2007). In the top-down approach, fluxes are inferred from atmospheric CO₂ measurements by means of an atmospheric transport model linking the measurements to fluxes upwind. The availability of abundant and accurate measurements and realistic transport models is key to the success of this approach (e.g., Enting et al., 1995). Consequently, large investments have been made in establishing reliable measurement networks, including in situ measurements of CO₂ concentrations from the surface, towers, and aircrafts (e.g., the NOAA ESRL Carbon Cycle Cooperative Global Air Sampling Network; Dlugokencky et al., 2013 and the Earth Networks Greenhouse Gas Network; <http://ghg.earthnetworks.com/>), and satellite missions dedicated to the measurement of CO₂ column amounts. The last include the Greenhouse gases Observing Satellite (GOSAT) launched in 2009 (Yokota et al., 2009), the Orbiting Carbon Observatory 2 (OCO-2) launched in 2014 (Crisp et al., 2008; Eldering et al., 2012), and the planned Active Sensing of CO₂ Emissions over Nights, Days, and Seasons (ASCENDS) mission recommended by the US National Academy of Sciences Decadal Survey (NRC, 2007).

The objective of our study is to quantify the ability of ASCENDS column measurements to constrain CO₂ fluxes top-down at relatively high resolution. The ASCENDS active measurement concept offers unique capabilities compared with passive satellite systems that rely on thermal emission or reflected sunlight (Kawa et al., 2010). These capabilities will enhance spatial and temporal coverage while providing high precision and accuracy. ASCENDS will extend coverage through its ability to sample between small cloud gaps and through thin clouds without interference. In addition, since a lidar-based system does not require the presence of the sun, it allows for observations of high-latitude regions during the winter. Measurements can be made both night and day, thereby reducing sampling bias due to (and potentially providing constraints on) diurnal variations in CO₂ fluxes driven by ecosystem respiration and primary production.

Global studies of the impact of satellite measurements on top-down estimates of CO₂ fluxes, beginning with the study by Rayner and O’Brien (2001), have established the benefit of using satellite measurements for constraining CO₂ fluxes at a precision level similar to or better than that provided by existing in situ networks. At present, these approaches estimate the reduction of flux uncertainties stemming from the availability of satellite data using an inverse solution for relatively coarse grid boxes or regions at weekly to monthly resolution (e.g., Houweling et al., 2004; Chevallier et al., 2007; Feng et al., 2009; Baker et al., 2010; Kaminski et al., 2010; Hungershofer et al., 2010; Basu et al., 2013; Deng et al., 2014). The present study extends these global studies to the regional scale using simulated ASCENDS data. Regional trace gas inversions are well suited for making use of high-density satellite observations to constrain fluxes at

fine scales. Regional transport models are less computationally expensive to run than global transport models for a given resolution, so it is more tractable to run a regional model at high resolution. The more precise determination of source-receptor relationships allows one to solve for fluxes at a finer resolution. This reduces potential “aggregation error” resulting from assuming fixed fine-scale flux patterns when optimizing scaling factors on a coarser scale (Kaminski et al., 2001; Engelen et al., 2002; Gerbig et al., 2003; Bocquet et al., 2011).

We use a novel approach for our inversions that facilitates high-resolution evaluation of satellite column measurements. The approach relies on a Lagrangian, or air-mass-following, transport model (as opposed to an Eulerian, or fixed-frame-of-reference, model), run backward in time from the observation points (receptors) using ensembles of particles to generate footprints describing the sensitivity of satellite CO₂ measurements to surface fluxes in upwind regions. Lagrangian particle dispersion models enable more precise simulation of transport in the near field than gridded transport models since, in the former, particle locations are not restricted to a grid and meteorological fields are interpolated to the subgrid-scale locations. Thus filamentation processes, for example, can be resolved (Lin et al., 2003), artificial diffusion over grid cells is avoided, and representation errors (Pillai et al., 2010) are minimized. The Lagrangian approach, implemented in the backward (receptor-oriented) mode, offers a natural way of calculating the adjoint of the atmospheric transport model. The utility of Lagrangian particle dispersion models is well established for regional trace gas flux inversions involving in situ observations (e.g., Gerbig et al., 2003; Lin et al., 2004; Kort et al., 2008, 2010; Zhao et al., 2009; Schuh et al., 2010; Göckede et al., 2010a; Brioude et al., 2011, 2012, 2013; Gourdji et al., 2012; Miller et al., 2012, 2013; McKain et al., 2012; Lauvaux et al., 2012). A convenient feature of Lagrangian footprints is their portability – they can be shared with other groups and readily applied to different flux models, inversion approaches, and molecular species, thus enabling comparisons based on a common modeling component. In addition, footprints for different measurement platforms can be merged easily in an inversion.

In this observing system simulation experiment (OSSE) we utilize the Stochastic Time-Inverted Lagrangian Transport (STILT) particle dispersion model (Lin et al., 2003), driven by meteorological fields from the Weather Research and Forecasting (WRF) model (Skamarock and Klemp, 2008) in a domain encompassing North America, in a Bayesian inversion. The WRF-STILT (Nehrkorn et al., 2010) footprints are used to compute weekly flux uncertainties over a 1° latitude × 1° longitude grid. This study focuses on land-based biospheric fluxes. We report results based on realistic sampling and observation errors for a set of ASCENDS instrument designs and other input data fields for the year 2007. Section 2 provides details on our inputs and inversion methods and presents examples of observation

uncertainties, a priori flux uncertainties, and WRF–STILT footprint maps. Section 3 presents posterior flux uncertainty results at various spatial and temporal scales, as well as comparisons with other studies. Section 4 discusses target and threshold requirements for instrument design parameters with respect to addressing key scientific questions. It also discusses sensitivity to additional sources of uncertainty and limitations of our analysis, as well as other considerations regarding ASCENDS. Section 5 contains concluding remarks.

2 Methods

2.1 Inversion approach

We use a Bayesian synthesis inversion method, which optimizes the agreement between model and observed CO₂ concentrations and a priori and a posteriori flux estimates in a least-squares manner (e.g., Enting et al., 1995). Since we focus on random error levels in constraining the fluxes using ASCENDS observations, we did not perform a full inversion and computed only the a posteriori flux error covariance associated with the inversion solution. The a posteriori flux error covariance matrix is given by

$$\hat{\mathbf{S}} = \left(\mathbf{K}^T \mathbf{S}_e^{-1} \mathbf{K} + \mathbf{S}_a^{-1} \right)^{-1}, \quad (1)$$

where

\mathbf{K} is the Jacobian matrix describing the sensitivity of concentrations to changes in the state vector elements (in this case, fluxes)

\mathbf{S}_e is the observation error covariance matrix

\mathbf{S}_a is the a priori flux error covariance matrix.

We directly solve for $\hat{\mathbf{S}}$, the square roots of the diagonal elements of which provide the estimates of the a posteriori flux uncertainties.

We solve for flux uncertainties in each land cell on a $1^\circ \times 1^\circ$ grid across North America (from 10° N to 70° N and from 170° W to 50° W). The time span is 5 weeks in each of the 4 seasons in 2007 (the first 4 weeks of January, April, July, and October plus the week preceding each of those months). We focus on weekly flux resolution in this study, rather than daily or higher resolution, for computational efficiency. In addition, the Decadal Survey called for a satellite mission that can constrain carbon cycle fluxes at a weekly resolution on 1° grids (NRC, 2007). The ASCENDS observations would likely also provide significant constraints on fluxes at higher resolutions (e.g., daily), as suggested by test inversions not reported here.

We solve Eq. (1) using the standard matrix inversion function in the Interactive Data Language (IDL) software package. We also verify the solution using the alternative singular value decomposition approach (Rayner et al., 1999) in IDL. Given the large dimensions of the matrices – more than

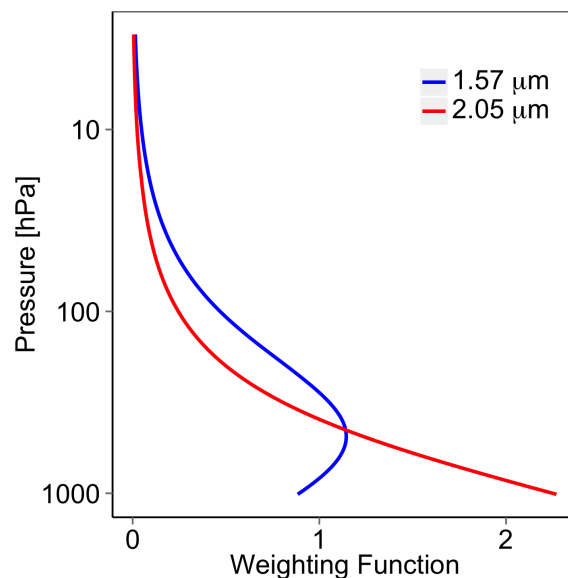


Figure 1. Vertical weighting functions per ppmv of CO₂ (10^{-6} ppmv⁻¹ hPa⁻¹) for two candidate ASCENDS wavelengths. These relate differential optical depth lidar measurements (on-line minus off-line) to column-average CO₂ mixing ratios. The precise on-line wavelengths used here are 1.571121 μ m, which is 10 picometers (pm) offset from line center, and 2.051034 μ m.

15 000 10 sec average observations each month and 13 205 weekly flux elements over each 5 week period – the procedure requires large amounts of computer memory but a modest amount of processing time: several hours per monthly inversion on the NASA Center for Climate Simulation high-performance computing system.

2.2 Observational sampling and simulated measurement uncertainties

We consider candidate lidar wavelengths near 1.57 μ m and 2.05 μ m (Caron and Durand, 2009). These have peak sensitivities in the mid- and lower troposphere, respectively (Fig. 1). Other candidate wavelengths with different vertical sensitivities and error characteristics are possible and could be assessed with the same inversion methodology. We derive the temporal–spatial sampling and random error characteristics for ASCENDS pseudo-data based on real cloud/aerosol and surface backscatter conditions for the year 2007 in a method similar to that of Kawa et al. (2010). Observation locations are taken from Cloud-Aerosol Lidar and Infrared Pathfinder Satellite Observation (CALIPSO) satellite orbit tracks. We use only locations that fall within the domain used in the WRF runs (Sect. 2.4), excluding those within 400 km of the boundaries in order to provide adequate WRF coverage to simulate back trajectory calculations inside the domain (Fig. 2). The errors are calculated as a function of optical depth (OD) measured by CALIPSO and surface backscatter calculated from Moderate Resolution Imaging Spectro-

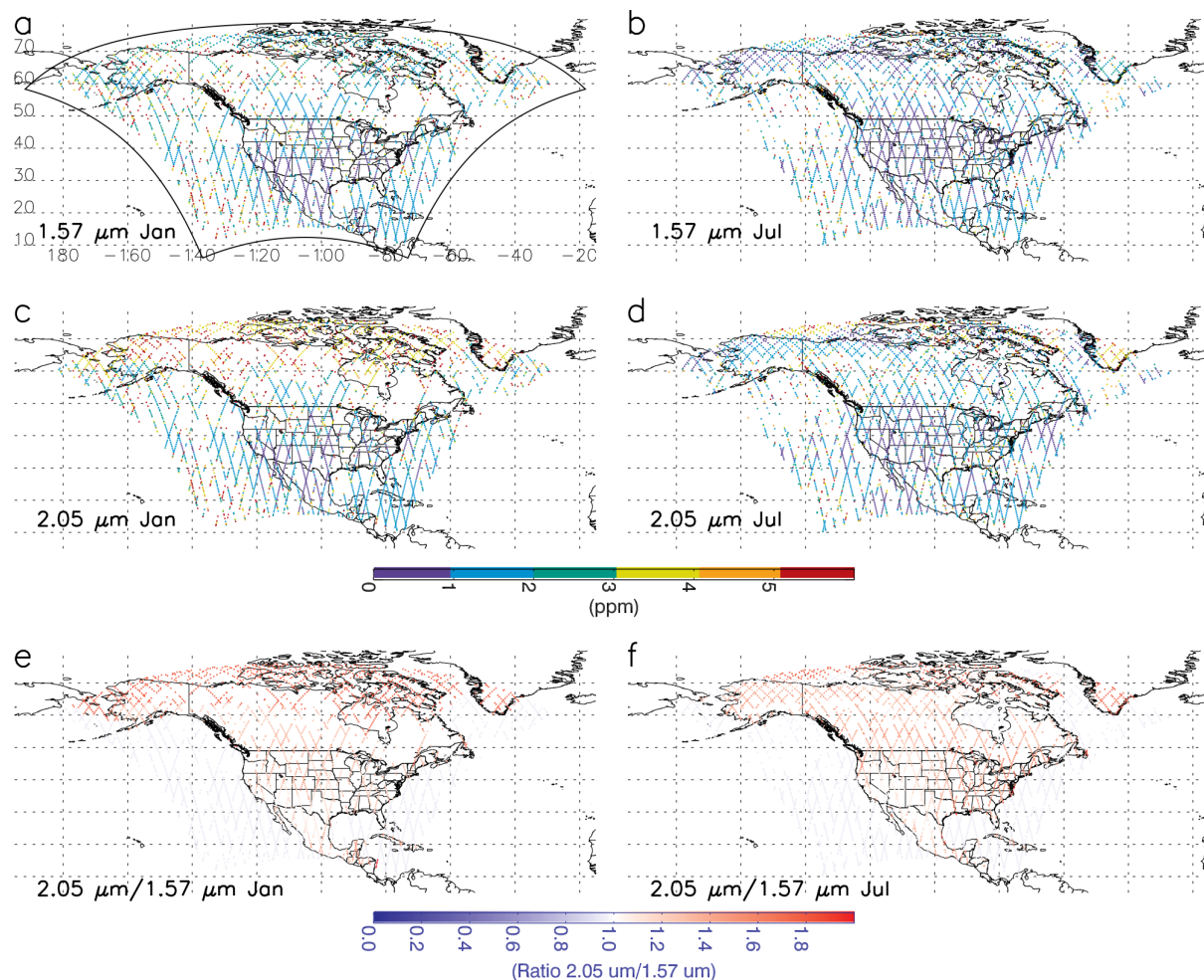


Figure 2. Examples of measurement locations (individual 10 sec averages) and 10 sec uncertainties (1σ) for the 0.5 ppm RRV random error case across 7-day spans for (a) the 1.57 μm wavelength in January and (b) in July; for (c) the 2.05 μm wavelength in January and (d) in July. Locations with OD > 0.7 are rejected. The uncertainty ratio of the 2.05 μm to 1.57 μm wavelength (e) in January and (f) in July. The WRF domain for the runs utilized in this study is indicated by the bold black lines in (a).

radiometer (MODIS) satellite reflectance over land or glint backscatter using 10 m analyzed wind speeds (Hu et al., 2008) interpolated to the sample locations over oceans. Samples with total column cloud plus aerosol OD > 0.7 are rejected. For each wavelength case, the measurement errors at each location are scaled to two possible performance levels: 0.5 ppm and 1.0 ppm error (10 sec average) under clear-sky conditions (cloud/aerosol OD = 0) for a reflectivity equal to that at a reference site, Railroad Valley (RRV), Nevada. The errors for each 5 km (0.74 sec) individual CALIPSO observation point are aggregated over 10 sec (67 km) intervals to increase signal-to-noise for pseudo-data using the formula

$$\sigma(10\text{ s}) = \sqrt{\frac{\sum_{i=1}^N \sigma(5\text{ km})_i^2}{N^2}},$$

where N is the number of valid 5 km observations across the 10 sec span. Such a 10 sec, conditionally sampled measurement is expected to represent the basic ASCENDS CO₂ data granule. The uncertainties in the series

of 10 sec pseudo-data are assumed to be uncorrelated, i.e., the observation error covariance matrix \mathbf{S}_e is diagonal.

Examples of the coverage of ASCENDS observations available for analysis and their associated uncertainties (for a reference uncertainty at RRV of 0.5 ppm) are shown in Fig. 2 over 7-day periods in January and July for the two candidate wavelengths. ASCENDS provides dense coverage over the domain with few large gaps, especially in July. A large majority of the 10-second-average observations have uncertainties of < 2 ppm in all four cases except for 2.05 μm in January. The uncertainties are especially small over land areas, which is helpful for constraining terrestrial fluxes. The uncertainties are generally larger for 2.05 μm than for 1.57 μm (by a factor of 1–1.6 over snow-free land and a factor of 1.6–1.8 over snow-/ice-covered areas) except in ice-free oceanic areas, where the uncertainties are similar (Fig. 2e and f).

Table 1. Spatiotemporal correlation parameters used.

Month	Spatial correlation e-folding length (km)	Temporal correlation e-folding length (days)
January	481	17.2
April	419	7.2
July	284	6.9
October	638	1.6

2.3 A priori flux uncertainties

We derived a priori flux uncertainties at $1^\circ \times 1^\circ$ resolution from the variability of net ecosystem exchange (NEE) in the Carnegie–Ames–Stanford Approach (CASA) biogeochemical model coupled to version 3 of the Global Fire Emissions Database (GFED3) (Randerson et al., 1996; van der Werf et al., 2006, 2010). CASA-GFED is driven by meteorological data from the Modern-Era Retrospective Analysis for Research and Applications (MERRA) (Rienecker et al., 2011). In the version of CASA used here, a sink of $\sim 100 \text{ Tg C yr}^{-1}$ is induced by crop harvest in the US Midwest, prescribed based on National Agriculture Statistics Service data on crop area and harvest. We neglected uncertainties in fossil fuel emissions, assuming like most previous inversion studies that those emissions are relatively well known. We ignored oceanic fluxes as well for this study since their uncertainties are also relatively small (e.g., Baker et al., 2010).

The a priori flux uncertainties were specifically derived from the standard deviations of daily mean CASA-GFED NEE over each month in 2007 divided by $\sqrt{7}$ to scale approximately to weekly uncertainties. This approach assumes that the more variable the model fluxes are in a particular grid cell and month, the larger the errors tend to be; the same reasoning has been applied in previous inversion studies to the estimation of model–data mismatch errors (e.g., Wang et al., 2008). We enlarged the resulting uncertainties uniformly by a factor of 4 to approximate the magnitude of those used in the global ASCENDS OSSE described in Sect. 3.2 of this paper; these are, in turn, essentially the same as the standard ones of Baker et al. (2010), based on differences between two sets of bottom–up flux estimates. In addition to allowing for better comparison of the two OSSEs, the enlargement by a factor of 4 is consistent with suggestions by biospheric model intercomparisons that the true flux uncertainty is greater than that based on a single model’s variability (Huntzinger et al., 2012).

Off-diagonal elements of the a priori flux error covariance matrix are filled using spatial and temporal error correlations derived from an isotropic exponential decay model with month-specific correlation lengths (Table 1) estimated from ground-based and aircraft CO₂ data in a North America regional inversion by Gourdji et al. (2012). Although these correlation lengths are not strictly applicable to our study, which

has a different setup from that in the geostatistical inverse modeling system of Gourdji et al. (2012), they are nonetheless reasonable estimates in general for the purposes of this study. Note that Gourdji et al. (2012) used a 3-hourly flux resolution, so the temporal correlation lengths may be too short for the coarser weekly resolution of our study. Chevallier et al. (2012) show that aggregation of fluxes to coarser scales increases the error correlation length. The analysis by Chevallier et al. (2012) using global flux tower data found a weekly-scale temporal error correlation length of 36 days, longer than the values we use. They found a spatial correlation length of less than 100 km at the site scale ($\sim 1 \text{ km}$), increasing to 500 km at a 300 km-grid scale; our correlation lengths (100 km grid) mostly fall within that range. In a test, we used alternative values for the spatiotemporal correlation lengths derived from the Chevallier et al. study and found that the inversion results are moderately sensitive (Sect. 4.2).

Our CASA-GFED-based a priori flux uncertainties, scaled to approximate the values used by Baker et al. (2010), are shown in Fig. 3. The largest uncertainties occur generally where the absolute value of NEE is highest, e.g., in the “Corn Belt” of the US in summer. The spatial and seasonal variations exhibit similarities to those of Baker et al. (2010).

2.4 WRF–STILT model, footprints, and Jacobians

The STILT Lagrangian model, driven by WRF meteorological fields, has features (including a realistic treatment of convective fluxes and mass conservation properties) that are important for accurate top–down estimates of GHG fluxes that rely on small gradients in the measured concentrations (Nehrkorn et al., 2010). In the present application of STILT (www.stilt-model.org, revision 640), hourly output from WRF version 2.2 is used to provide the transport fields over a North American domain at a resolution of 40 km horizontally and 31 eta levels vertically (Fig. 2a). Meteorological fields from the North American Regional Reanalysis (NARR) at 32 km resolution are used to provide initial and boundary conditions for the WRF runs. To prevent drift of the WRF simulations from the analyses, the meteorological fields (horizontal winds, temperature, and water vapor at all levels) are nudged to the NARR analysis every 3 h with a 1 h relaxation time and are reinitialized every 24 h (at 00:00 UTC). Simulations are run out for 30 h, but only hours 7–30 from each simulation are used to avoid spin-up effects during the first 6 h. The WRF physics options used here are the same as those described by Nehrkorn et al. (2010).

A footprint quantitatively describes how much surface fluxes originating in upwind regions contribute to the total mixing ratio at a particular measurement location; it has units of mixing ratio per unit flux. This is to be distinguished from a satellite footprint, which is the area of earth reflecting the lidar signal. In the current application, footprints are computed for each 5 km simulated observation that passes the cloud/aerosol filter in January, April, July, and October

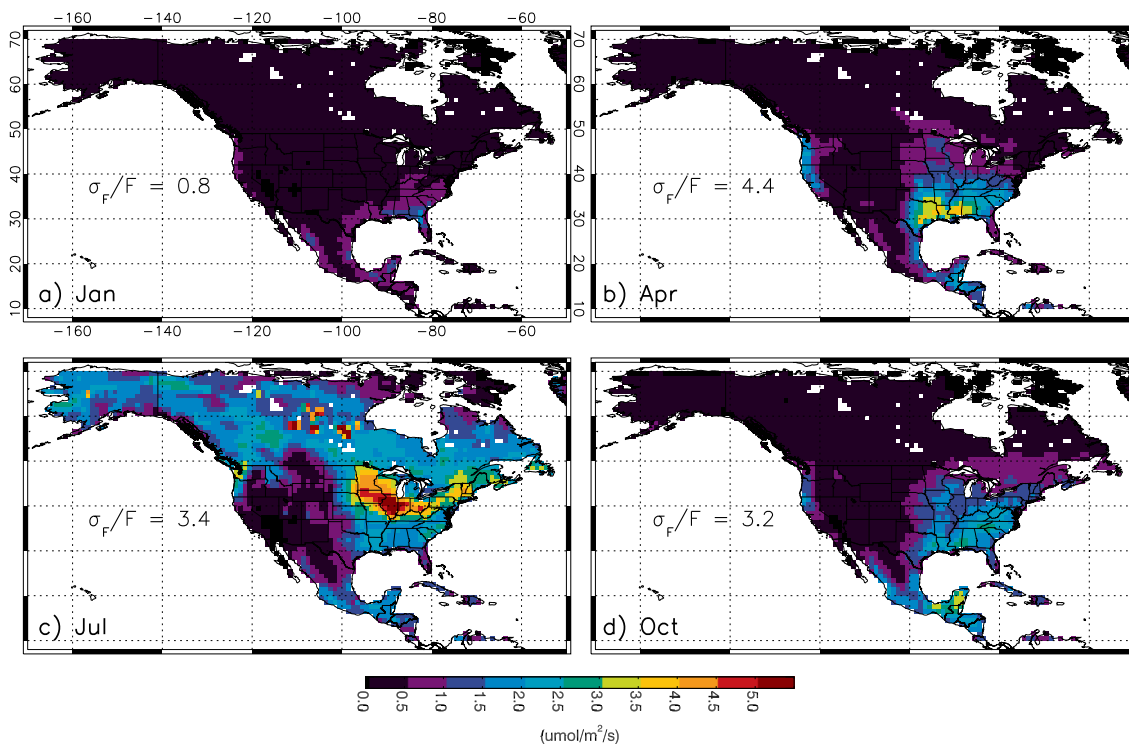


Figure 3. A priori weekly flux uncertainty for (a) January, (b) April, (c) July, and (d) October. Average fractional flux uncertainties over the domain are given in each panel (where F is flux). $1 \mu\text{mol m}^{-2} \text{s}^{-1} = 1.037 \text{ g C m}^{-2} \text{ d}^{-1} = 4.4 \times 10^{-8} \text{ kg CO}_2 \text{ m}^{-2} \text{ s}^{-1}$.

2007 at 3 h intervals back to 10 days prior to the observation time. Separate footprint maps have been computed for 15 receptor positions above ground level for the purpose of vertically convolving with the lidar weighting functions and producing one weighted-average footprint per measurement. The receptors are spaced 1 km apart in the vertical from 0.5 to 14.5 km a.g.l. This procedure results in $\sim 90\,000$ footprint calculations per day, placing stringent demands on our computational approach. In this study, STILT simulates the release of an ensemble of 500 particles at each receptor in the column.

It is important to note that although a footprint is defined for each of the 15 vertical levels, the footprint expresses the sensitivity of the mixing ratio (measured at the receptor point located at that vertical level) to the surface fluxes upwind, not to the fluxes upwind at the same level. Thus the footprints defined for receptor points located at high altitudes (e.g., 12.5, 13.5, 14.5 km) are often zero, indicating that a receptor at that upper level is not influenced by surface fluxes inside the domain (within the 10-day span examined here). Conversely, receptor points located at the lowest levels (e.g., 0.5, 1.5, 2.5 km) tend to have large footprints (with values of the order of $10^{-3} \text{ ppm}/(\mu\text{mol m}^{-2} \text{ s}^{-1})$ or higher), being most influenced by nearby surface fluxes.

Figure 4 shows the vertically-weighted footprints of a selected column measurement location (in southern Canada) over 10 days for the 1.57 and 2.05 μm wavelengths. Non-

zero footprints occur wherever air observed at the receptor site has been in contact with the surface within the past 10 days. Patterns of vertical and horizontal atmospheric motion explain the somewhat unexpected spatial patterns of the footprints in this particular example, with very high values occurring at a significant distance upwind of the receptor (in the vicinity of Texas and Oklahoma) as well as immediately upwind. Vertical mixing lifts the signature of surface fluxes to higher levels so it can be detected by receptors at multiple levels, resulting in a higher value for the vertically convolved footprint; slower winds in a particular area, such as Texas and Oklahoma, can result in a larger time-integrated impact of fluxes on the observation. The footprint values are larger for 2.05 μm due to the higher sensitivity of that measurement near the surface, as previously discussed.

To construct the Jacobians, \mathbf{K} , that enter Eq. (1), we averaged the footprints of all the 5 km receptor locations within a given 10 sec averaging period along the satellite track, including only the land cells. We arranged the averaged footprints in a two-dimensional Jacobian, running across flux time intervals and grid cells in one direction and across observations in the other (the 3 h flux intervals associated with each transport run are defined relative to fixed UTC times and not relative to the observation times). We then aggregated the Jacobian elements to the final flux resolution, e.g., weekly. For any particular month, we solved only for fluxes

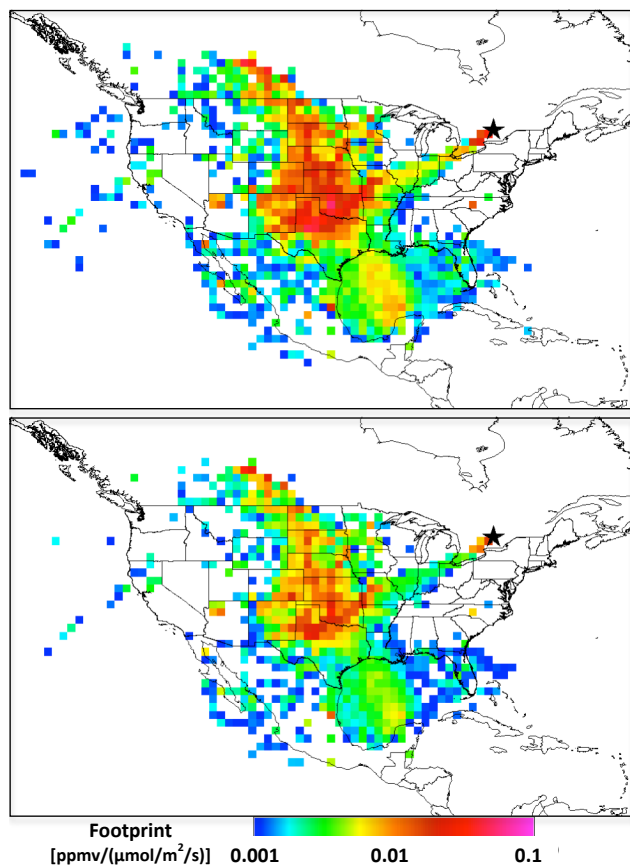


Figure 4. Footprint maps for one simulated ASCENDS measurement location (marked by black star) on 1 January 2007 at 18:00 UTC, integrated over 10 days and convolved over the 500–14 500 m AGL range with two candidate ASCENDS weighting functions: the CO₂ laser lines at 2.05 μm (top) and 1.57 μm (bottom). Note that the native temporal resolution of the footprints is 3 h; the 10-day integral in this figure is for illustrative purposes only. Only footprints over land are used in the analysis.

occurring in the week prior to the beginning of the month and in the first 4 weeks of that month.

Figure 5 shows the overall influence of the surface fluxes on the observations during each month (i.e., the average weekly Jacobian values for the 1.57 μm weighting function). Values tend to decrease from west to east, reflecting the general westerly wind, which transports CO₂ influences out of the domain more quickly for fluxes occurring closer to the eastern edge than for those farther west. Values also tend to decrease towards the north and northwest and in the southernmost part of the continent; these areas lie close to the edges of the domain shown in Fig. 2a. Areas with smaller average footprint values are generally not as well constrained by the observations, as will be discussed later in this paper; thus, our domain boundaries artificially limit flux constraints in certain parts of the continent. Previous regional inversion studies may not have highlighted this issue because they used

ground-based observations, whose sensitivities are more confined to near-field fluxes than those of satellite column measurements. We will quantify the impact of the boundaries on average footprint gradients in future work, providing guidance for future studies on optimal sizes and shapes of domains (e.g., shifted eastward) to avoid large gradients while controlling computational cost.

Footprint values are largest in summer due once again to horizontal and vertical motions. Winds during this season are relatively light and allow the fluxes to stay inside the domain for a long time, maximizing their integrated influence on observations in the domain; vertical mixing across the deep boundary layer brings particles over a large portion of the column into contact with the surface.

Although WRF-STILT provides the capability to generate and optimize boundary condition influences on observed concentrations, this was not available at the time of this study and, consequently, we neglect uncertainties in the influence of boundary conditions in our standard inversion (discussed further in Sect. 4.2). Similarly, we neglect uncertainties regarding the influence of North American fluxes occurring more than 10 days before a particular observation. Note that fluxes are often transported out of the domain within 10 days, so that these fluxes can only influence the observations via the boundary conditions.

3 Results

In the following, we present results for four cases involving different combinations of measurement wavelength and baseline error level: 1.57 μm and 0.5 ppm RRV error (case 1), 1.57 μm and 1.0 ppm (case 2), 2.05 μm and 0.5 ppm (case 3), and 2.05 μm and 1.0 ppm (case 4).

3.1 A posteriori flux uncertainties at the grid level

A posteriori uncertainties (Fig. 6) are smaller than the a priori values (Fig. 3), an expected result of the incorporation of observational information. The reduction in uncertainty is often larger in areas that have higher a priori uncertainties, as can be seen more clearly in the maps of percentage reduction in uncertainty in Fig. 7. Uncertainty reductions are relatively large year-round in places such as southern Mexico and the Pacific Northwest of the US; in April and October in the southeastern US; and in July in the US Midwest, areas with forest fire emissions in central Canada (appearing as hot spots of uncertainty reduction), and Alaska and western Canada. A priori uncertainties are relatively high in these areas so that there is more room for observations to tighten the constraint. In contrast, where a priori uncertainties are already small, observations are not able to provide a much tighter constraint.

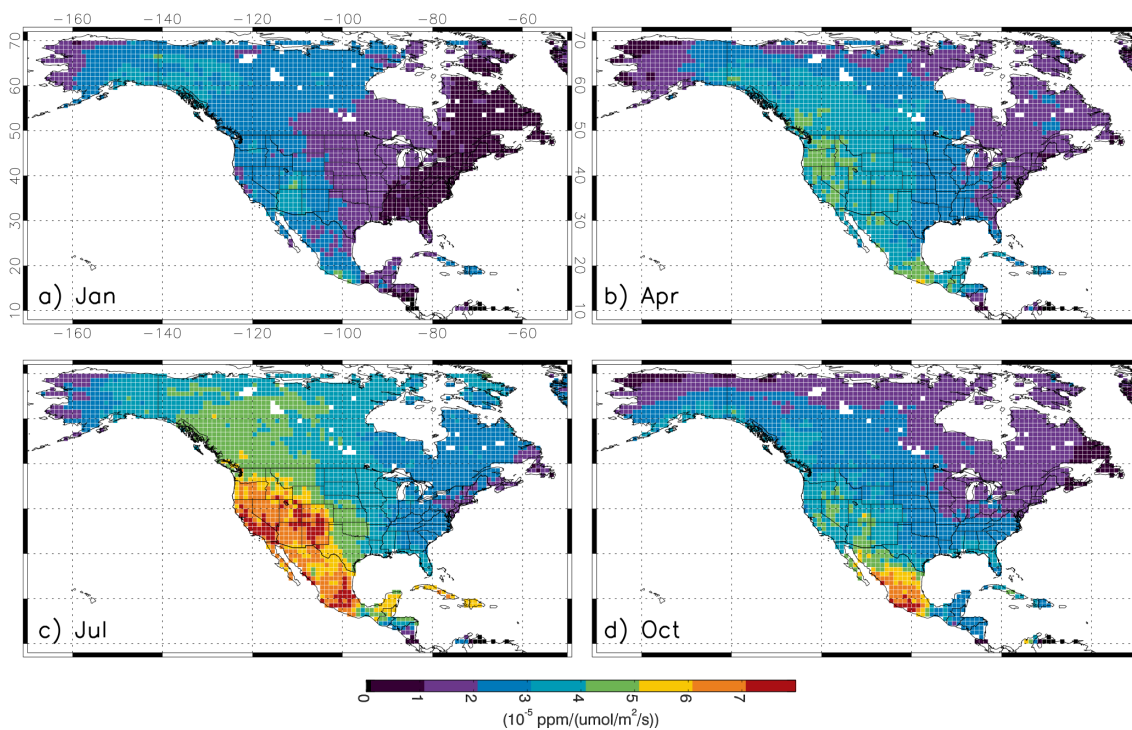


Figure 5. Jacobian values averaged over all observations and weekly flux intervals for the 1.57 μm weighting function in (a) January, (b) April, (c) July, and (d) October.

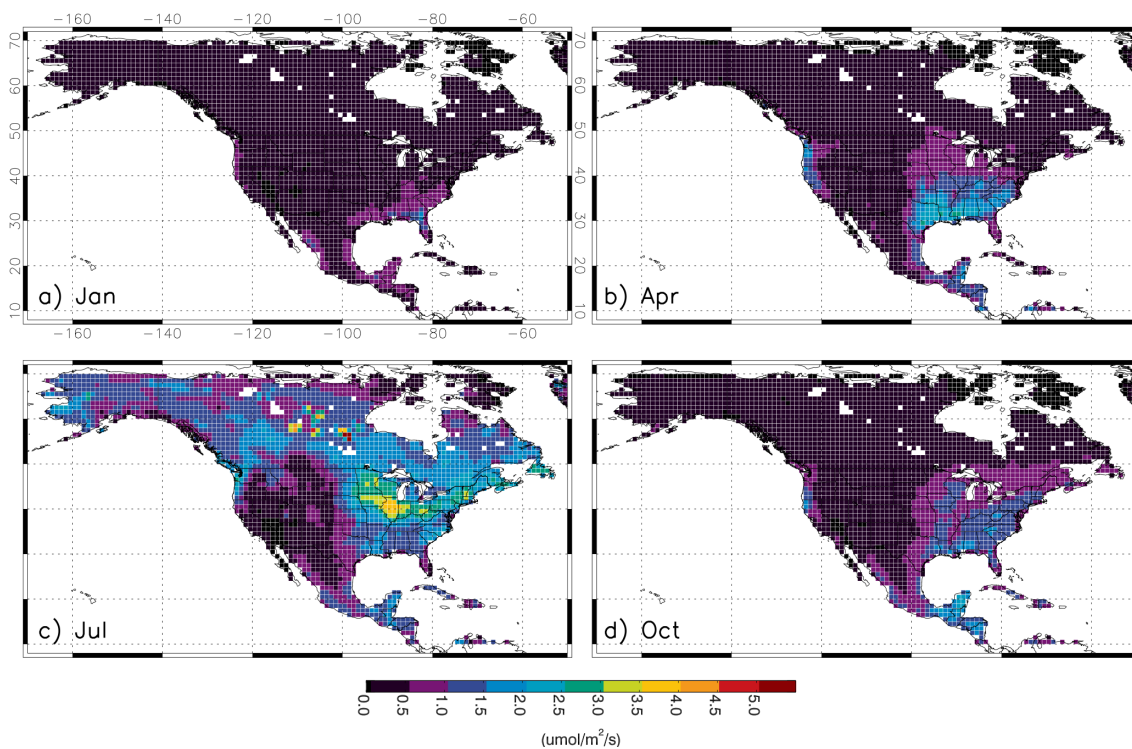


Figure 6. A posteriori weekly flux uncertainty during (a) January, (b) April, (c) July, and (d) October, for case 1 (1.57 μm and 0.5 ppm RRV error). Shown here are RMS values from the first 4 weeks of each month. $1 \mu\text{mol m}^{-2} \text{s}^{-1} = 1.037 \text{ g C m}^{-2} \text{ d}^{-1} = 4.4 \times 10^{-8} \text{ kg CO}_2 \text{ m}^{-2} \text{ s}^{-1}$.

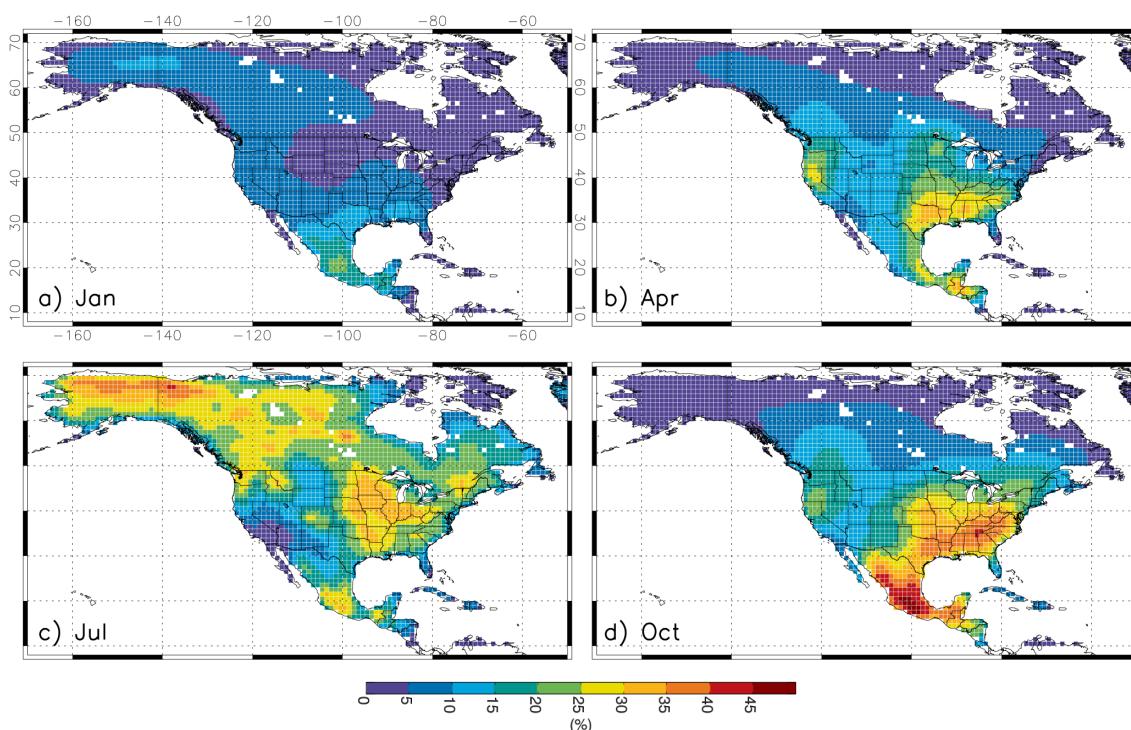


Figure 7. Weekly fractional flux uncertainty reduction over (a) January, (b) April, (c) July, and (d) October, for case 1 (1.57 μm and 0.5 ppm RRV error). Shown here are results from the first 4 weeks of each month.

Of course, the uncertainty reductions are not dependent simply on the prior uncertainties. For example, the highest uncertainty reductions, up to 50 %, occur in southern Mexico in October, where a priori uncertainties are not especially large. The high uncertainty reductions here can be explained by the large Jacobian values (Fig. 5) combined with the low uncertainties of nearby observations (not shown). Although a priori uncertainties and Jacobian values in July in this area are similar to those in October, observation uncertainties are higher, resulting in lower uncertainty reductions. The tendency of uncertainty reductions to be higher where average Jacobian values are larger can also be seen in the similarity of the spatial patterns in the January maps in Figs. 5a and 7a, for example. As described in Sect. 2.4, fluxes in western and central areas of the continent are captured by more observations in the domain than fluxes in the east and close to the other edges; thus, the former can be better constrained in this inversion.

In July, the largest uncertainty reductions occur in northern Alaska and northwestern Canada, which have much smaller a priori uncertainties than places such as the Midwest. This is an effect of the smaller grid cells at higher latitudes: the a priori errors are correlated over larger numbers of cells at these latitudes given the spatially uniform correlation lengths we specify, so that the average flux over each cell is more tightly constrained than that for an otherwise comparable cell at lower latitudes. This is a less important issue when results

are aggregated to the larger scales dealt with in later sections of this paper.

Uncertainty reductions are smallest in January, for the following reasons: (1) a priori flux uncertainties are smallest during the dormant season, (2) observation errors are largest in winter due to the low reflectance of snow and ice cover at the measurement wavelengths, and (3) there is fast dispersion of fluxes in winter by strong winds, transporting fluxes out of the domain and out of detection by observations in the domain and thus reducing the average Jacobian values in January relative to the other months (Fig. 5). The ratio of the averaged Jacobian elements for January to those for July is 0.51 for the 1.57 μm wavelength.

Inversions for the 2.05 μm wavelength, with its higher sensitivity near the surface, result in greater uncertainty reduction despite the larger observation errors over land (Fig. 8c vs. 8a, and 8d vs. 8b). Inversions assuming 1.0 ppm instead of 0.5 ppm error at RRV result in less uncertainty reduction (Fig. 8b vs. 8a, and 8d vs. 8c) as expected, with maximum uncertainty reduction of $\sim 30\%$ vs. $\sim 40\%$, for 1.57 μm . These cases are compared further in the section below on biome-aggregated results.

3.2 Results aggregated to biomes and continent, and compared with other inversion systems

For assessing large-scale changes in carbon sources and sinks it is useful to aggregate high-resolution results to biomes and

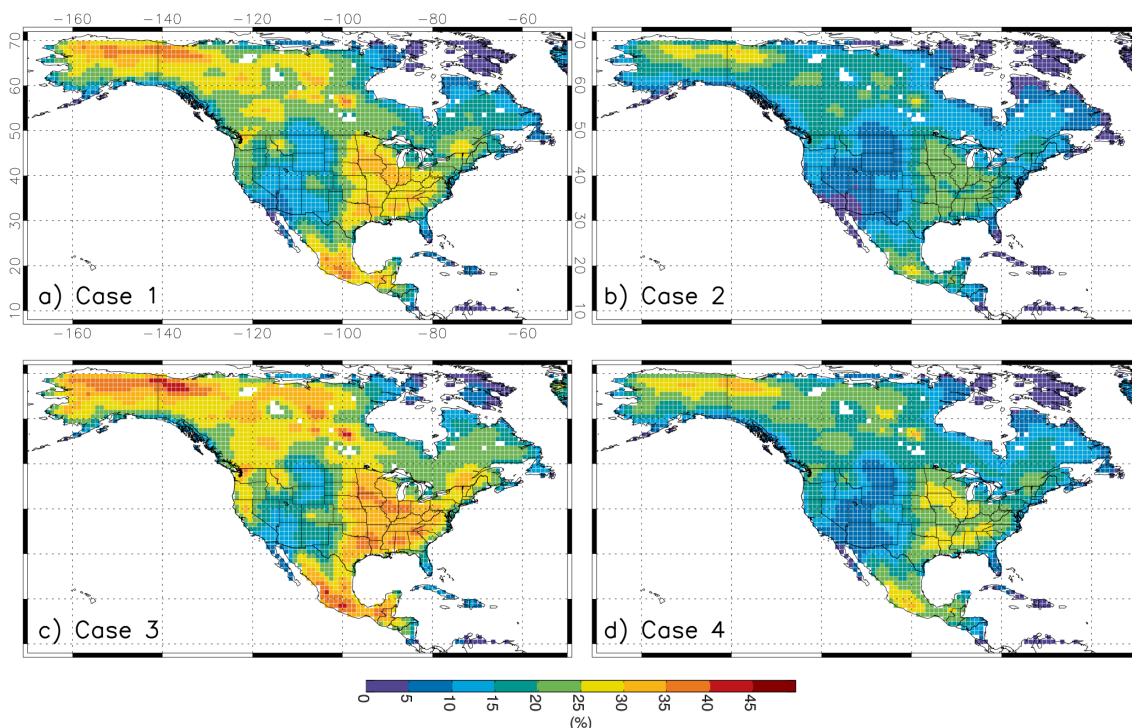


Figure 8. Weekly fractional flux uncertainty reduction (RMS over the 4 months) for (a) case 1 (1.57 μm and 0.5 ppm RRV error), (b) case 2 (1.57 μm and 1.0 ppm), (c) case 3 (2.05 μm and 0.5 ppm), and (d) case 4 (2.05 μm and 1.0 ppm).

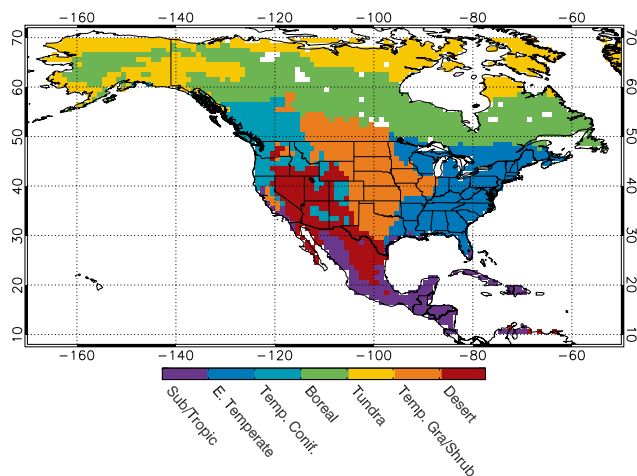


Figure 9. Biomes used, taken from Olson et al. (2001) with modifications by Gourdjji et al. (2012).

the entire continent, and to seasons and years. We use the biome definitions in Fig. 9 taken from Olson et al. (2001) with modifications by Gourdjji et al. (2012). To aggregate the flux uncertainties we summed up the variances within each biome and over each month and then the year, in units of $(\text{Pg C yr}^{-1})^2$, as well as the error covariances between grid cells and weeks.

We compare our results with those from two other inversion systems: a global inversion using ASCENDS observations (a companion study to this one) and a North American regional inversion using the same WRF–STILT Lagrangian model as ours but with a network of ground-based observation sites (Gourdjji et al., 2012). The global OSSE uses the same ASCENDS data set sampling and underlying observation error model as the regional OSSE. Among the primary differences are the global domain of the analysis (and thus the use of observations outside and inside the North American domain) and the coarser spatial resolution of the transport and flux solution, 4.5° latitude \times 6° longitude. Other differences include the mathematical technique of the inversion (variational data assimilation, as in an earlier study by Baker et al., 2010), the Eulerian transport model (PCTM; Kawa et al. 2004), the spatial patterns of the a priori flux uncertainties (the overall magnitudes are not different, as described in Sect. 2.3), the assumption of zero a priori error correlations, and the use of (estimate–truth) statistics as a proxy for flux uncertainty (Baker et al., 2010), given that the variational method does not directly compute a full a posteriori error covariance matrix. We aggregated the global inversion results to the same biomes, summing the (estimate–truth) values and accounting for fractional biome coverage in each of the coarse grid cells. Gourdjji et al. (2012) used a set of ground-based and aircraft measurements and a geostatistical inverse model to solve for biospheric fluxes and their

uncertainties at a $1^\circ \times 1^\circ$, 3-hourly resolution in 2004. We present these comparisons mainly to provide context for our results rather than to quantitatively analyze effects of various methodological differences.

Uncertainty reductions are largest in July and smallest in January at the continental scale (Table 2). The uncertainty reductions for the $1.57\ \mu\text{m}$ wavelength are on average 8 % smaller than those for $2.05\ \mu\text{m}$. The uncertainty reductions for the $1.57\ \mu\text{m}$ wavelength with 0.5 ppm error are larger than those for $2.05\ \mu\text{m}$ with 1.0 ppm error. The uncertainty reductions for 0.5 ppm error are on average 16 % larger than those for 1.0 ppm error.

At the annual biome scale our uncertainty reductions range from 50 % for the desert biome (averaged across the cases) to 70 % for the temperate grassland/shrubland biome (Fig. 10c). The reductions scale, as before, with increasing a priori uncertainty (Fig. 10a), observation quality and density, and now with the biome area (Fig. 10d). We find a modest correlation between uncertainty reduction and area in the set of biomes, with a linear correlation coefficient of 0.5. In addition, the uncertainty reduction is higher on the continental scale than on the biome scale. The a posteriori uncertainty increases with increasing area more slowly than does the a priori uncertainty because many of the a posteriori error covariance terms summed in the aggregation to biome are negative, whereas all of the a priori error covariance terms are positive or zero. This explains why uncertainty reduction tends to increase with increasing area.

Our a posteriori uncertainties range from 0.12 to $0.33\ \text{Pg C yr}^{-1}$ at the monthly continental scale across all four cases (Table 2), from 0.04 to $0.08\ \text{Pg C yr}^{-1}$ at the annual continental scale (Fig. 10a), and from 0.01 to $0.06\ \text{Pg C yr}^{-1}$ at the annual biome scale (Fig. 10a). To put these numbers into perspective, the estimated current global terrestrial sink is roughly $2.5\ \text{Pg C yr}^{-1}$ (Le Quéré et al., 2012). Our uncertainties are generally similar to those from the North American regional inversion of Gourdji et al. (2012) (Fig. 10a) and the global inversion (Fig. 10b), a notable exception being the overall continental result of Gourdji et al. (2012). Our a posteriori uncertainty for North America is small compared to Gourdji et al. (2012) likely because of the greater spatial coverage of ASCENDS as compared to the in situ network; some of the biomes are not well constrained by the in situ network (i.e., the ones for which Gourdji et al., 2012 did not report aggregated results). Note that the comparison is not totally consistent, given the methodological differences. The global inversion method for estimating uncertainties based on (estimate-truth) statistics cannot provide an annual uncertainty estimate for the one-year inversion and produces somewhat noisy results for individual months. Thus to compare the regional and global inversions we took the RMS of the four monthly uncertainties. The uncertainty reduction for our regional inversion is similar on average to that of the global inversion for case 1, across biomes and the entire continent (Fig. 10c), with continent-level values of 78 %

and 72 %, respectively. There are larger differences between the regional and global inversions for particular biomes. Although differences in prior uncertainties (Fig. 10b) could possibly explain the differences in uncertainty reduction for some of the biomes (subtropical/tropical, eastern temperate, temperate coniferous, desert), they do not for the others (boreal, tundra, temperate grassland/shrubland), suggesting that prior uncertainties are not the only factor producing the spatial pattern in the comparison.

4 Discussion

4.1 Target and threshold requirements

We now discuss the implications of our analysis for the ASCENDS design. Hungershofer et al. (2010) suggested levels of posterior flux uncertainty on different spatiotemporal scales that global CO₂ measurement missions should strive for in order to answer key carbon cycle science questions. In the following we evaluate our results relative to those requirements, the only such specific guidelines for CO₂ satellite missions in the scientific literature.

Hungershofer et al. suggested that to determine the location of the global terrestrial C sink and whether C cycle feedbacks are occurring one requires annual net carbon flux estimates with a precision better than $0.1\ \text{Pg C yr}^{-1}$ (threshold) or $0.02\ \text{Pg C yr}^{-1}$ (target) at a scale of $2000 \times 2000\ \text{km}$, similar to the biomes we consider. These precision levels are based on the range of estimated fluxes across various biomes. The proposed A-SCOPE active CO₂ measurement mission defined a similar target requirement: $0.02\ \text{Pg C yr}^{-1}$ at a scale of $1000 \times 1000\ \text{km}$ (Ingmann et al., 2008). According to our results (Fig. 10a) all tested ASCENDS cases would meet the minimum threshold requirement across all biomes easily, with a posteriori uncertainties ranging from 0.01 to $0.06\ \text{Pg C yr}^{-1}$. In addition, the two cases with 0.5 ppm error would meet the more stringent target requirement for a majority of biomes, while the two cases with 1.0 ppm error would meet it for 3 out of 7 biomes. The meeting of the target requirement is a consequence of the information provided by the observations and not merely an effect of the specified a priori uncertainty, given that the a priori uncertainty is higher than the target level for all biomes excepting desert (the prior uncertainty of which is already at the target level). One measure of the contribution of the observations to meeting the target is shown in Fig. 10e, which is a plot of the fractional uncertainty reduction necessary for different biomes to meet the target. The amounts are mostly greater than 50 %, reaching 85 % for eastern temperate.

4.2 Sensitivity tests: boundary conditions, a priori uncertainties, and correlation lengths

A simplifying assumption in our standard inversion is the neglect of uncertainties in the boundary conditions (BCs). It

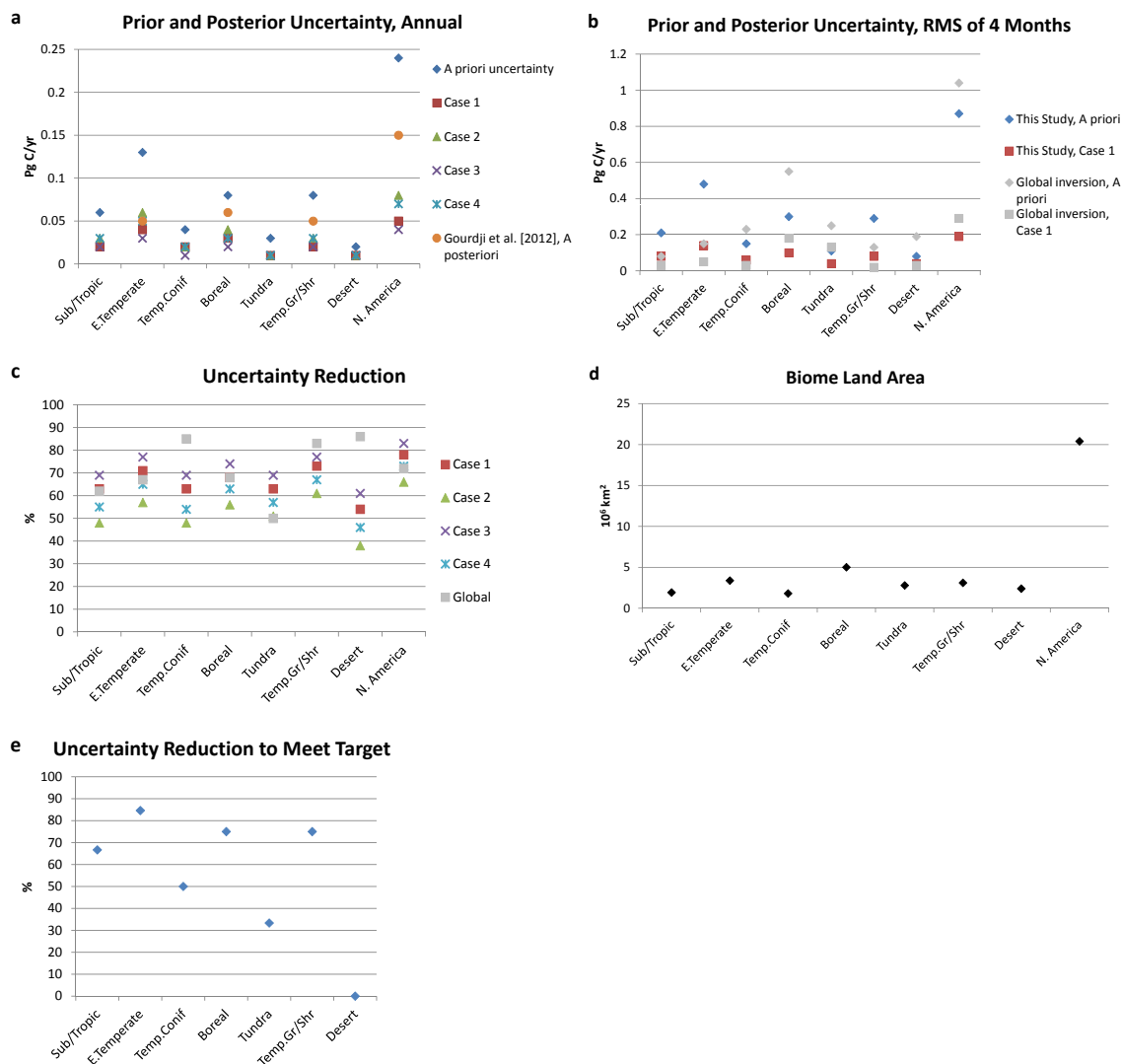


Figure 10. Results aggregated to biomes and continent and compared with other studies. **(a)** A priori and a posteriori uncertainties for the year, including results from Gourdji et al. (2012). **(b)** RMS of the four monthly uncertainties, including results from the global inversion. **(c)** Fractional uncertainty reductions. **(d)** Land area of the biomes. **(e)** Fractional uncertainty reduction necessary to meet the target requirement. Gourdji et al. (2012) reported results for only the three biomes that were well constrained by their in situ observation network, along with results aggregated over the full continent; we show the approximate average of their “Simple” and “NARR” inversions. The figure does not include a priori uncertainties for Gourdji et al. (2012) since their method does not rely on a priori estimates.

is especially important in a regional inversion (Eulerian or Lagrangian) to accurately account for the influence of lateral boundary inflow on concentrations within the domain (Göckede et al., 2010b; Lauvaux et al., 2012; Gourdji et al., 2012). Because we neglect BC uncertainties, we essentially assume that all of the information in the ASCENDS observations can be applied to reducing regional flux uncertainties rather than the combination of BC and flux uncertainties. Thus the amount of flux uncertainty reduction reported for our standard inversion may be higher than it would be if we accounted for BC uncertainties.

We conducted a test inversion for July (1.57 μm and 0.5 ppm error case) in which BCs are added as param-

eters (specifically, weekly average CO₂ mixing ratios over each of the four lateral walls of the domain) to be estimated in the state, with corresponding elements added to the Jacobian. Given that the actual Jacobian values are not available, we prescribed values that are somewhat realistic: 0.5 ppm ppm⁻¹ if an observation occurs in the same week as or after a BC, and 0 if an observation occurs before a BC. We assumed a priori uncertainties of 1 ppm for the BC, with no correlations among BC uncertainties or between BC and flux uncertainties. As expected, the reductions in flux uncertainty are smaller than the ones reported above, although the differences are only a factor of 0.01 or less. Weekly uncertainties for the BCs are reduced by 7–13%. A different experimen-

Table 2. Flux uncertainties aggregated to entire continent and month or year (Pg C yr⁻¹).

	January	April	July	October	Annual
Standard inversion					
A priori	0.42	0.78	1.26	0.82	0.24
A posteriori (uncertainty reduction)					
Case 1	0.24 (43 %)	0.17 (78 %)	0.15 (88 %)	0.2 (76 %)	0.05 (78 %)
Case 2	0.33 (21 %)	0.28 (65 %)	0.26 (80 %)	0.31 (61 %)	0.08 (66 %)
Case 3	0.18 (57 %)	0.13 (83 %)	0.12 (91 %)	0.15 (81 %)	0.04 (83 %)
Case 4	0.28 (35 %)	0.22 (72 %)	0.2 (84 %)	0.25 (69 %)	0.07 (73 %)
Inversion with alternative correl. lengths (200 km, 35 days)					
A priori	0.23	0.59	1.27	0.59	0.21
A posteriori (uncertainty reduction)					
Case 1	0.17 (25 %)	0.15 (74 %)	0.14 (89 %)	0.16 (73 %)	0.04 (80 %)

tal setup (e.g., larger Jacobian values for the BCs or a larger number of disaggregated BC parameters) could potentially result in a much larger effect on the flux uncertainty reductions.

In addition to containing random errors, BCs can also be a source of systematic errors. For example, Gourdj et al. (2012) found that two plausible sets of BC around North America generated inferred fluxes that differed by 0.7–0.9 Pg C yr⁻¹ on the annual continental scale (which is a very large amount compared to the annual a posteriori uncertainties for North America of 0.04–0.08 Pg C yr⁻¹ that we estimated in our OSSE; Fig. 10a). They concluded that BC errors may be the primary control on flux errors in regional inversions at this coarse scale, while other factors such as flux resolution, priors, and model transport are more important at subdomain scales.

Sparseness of observations has been a major cause of uncertainty in the boundary influence in previous regional inversions. Lauvaux et al. (2012), who conducted mesoscale inversions for the US Midwest using tower measurements, found BC errors to be a significant source of uncertainty in the C budget over 7 months. They estimated that a potential bias of 0.55 ppm in their BCs translates into a flux error of 24 Tg C over 7 months in their 1000 km × 1000 km domain. Although they applied corrections to the model-derived BCs using weekly aircraft profiles at four locations near their domain boundaries, they stated that the BC uncertainties were still large given the limited duration (a few hours per week) and spatial extent of the airborne observations, and concluded that additional observations would be necessary to reduce the uncertainties. ASCENDS is promising in this respect, as it (along with other satellites) will provide more frequent and widespread observations of concentrations at regional boundaries, possibly reducing the role of BCs in the overall C budget uncertainty to a minor one. ASCENDS observations could specifically be used in a global

CO₂ data assimilation system to provide accurate BCs for the regional flux inversion.

Posterior uncertainties are generally sensitive to the assumed prior uncertainties, although one might not expect the sensitivity to be so great in the case of a dense observational data set such as the one examined here. We test this hypothesis with an alternative prior uncertainty estimate, one that is uniformly larger than that of the standard inversion by a factor of 2. Figure 11a–d shows the ratio of the posterior uncertainty of the large-prior inversion to that of the standard inversion, normalized by a factor of 2. Large areas of the domain have ratios significantly less than 1, especially in July and October. Where the ratio is close to 1, the posterior uncertainty is sensitive to the prior, indicating that the observations have a relatively weak influence; where the ratio is significantly less than 1, the posterior uncertainty is not so sensitive to the prior. The test demonstrates that the posterior uncertainty in many areas is not highly sensitive to the prior uncertainty and is strongly influenced by the observations. However, the sensitivity is high in the tundra and the desert due to the tight (small) prior constraints in those regions (Fig. 3).

Although the posterior uncertainty is not highly sensitive to the prior in all areas, it still increases everywhere in the large-prior inversion relative to the standard inversion, implying that our findings regarding whether or not the observations meet the target requirement (Sect. 4.1) are dependent on the assumed priors. However, our standard priors are already enlarged uniformly by a factor of 4 relative to one set of prior uncertainty estimates, and they would have to be enlarged further over large areas to substantially increase biome-level posterior uncertainties. In addition, the larger the prior uncertainties are, the larger the uncertainty reductions are in general. Wherever the posterior uncertainty increases by a factor smaller than the prior uncertainty does (e.g., where the ratio is less than 1 in Fig. 11), the uncertainty reduction increases. Altogether, the results of this sensitivity test suggest that it

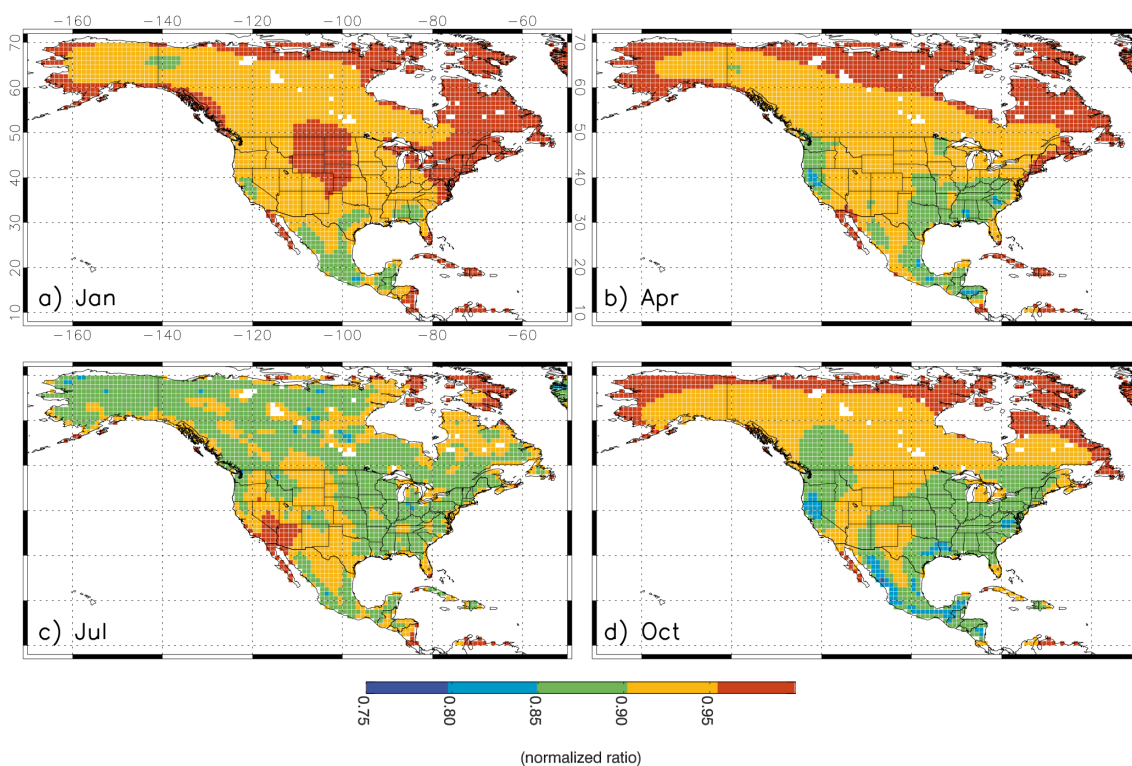


Figure 11. Ratio of the posterior uncertainty for the $2 \times$ prior inversion to that for the standard inversion, normalized by a factor of 2 for case 1 in (a) January, (b) April, (c) July, and (d) October.

is important to consider different measures of the impact of observations on flux estimates, such as posterior uncertainty and uncertainty reduction, as we have done in this OSSE, given that different measures can be affected differently by assumptions such as prior uncertainties.

The inversion results are potentially sensitive to the assumed a priori flux error correlation lengths, with longer correlation lengths leading to smoother uncertainty reduction patterns and larger uncertainty reductions. Rodgers (2000) shows that the inclusion of a priori error correlations can result in more “degrees of freedom for signal,” i.e., more information provided by the measurements on the unknowns. We carried out a test with alternative values for the correlation lengths derived from the study by Chevallier et al. (2012): a shorter spatial correlation length of 200 km and a longer temporal correlation length of 35 days for all months (we estimated these values from Fig. 5a and b of Chevallier et al. for the ~ 100 km and 7 day aggregation of our inversion). The resulting uncertainty reductions are smaller everywhere than those in our standard inversion at the grid scale, with values of up to 40 % in July and up to 15 % in January for case 1 (compared to 45 % and 25 %, respectively, in the standard inversion). Apparently, the decrease in the spatial correlation length relative to the standard inversion has a larger effect than the increase in the temporal correlation length. Aggregated to the continent and month, the uncertainty reduction is

less than that for the standard inversion for all months except July, for which the uncertainty reduction is marginally larger (Table 2). For July, the impact of the much longer temporal correlation length relative to the standard inversion on the aggregated result more than offsets that of the slightly shorter spatial correlation length. The annual uncertainty reduction of the alternative inversion is slightly larger than that of the standard inversion because of the disproportionate influence of the large a priori uncertainty of July. We conclude that our inversion results vary moderately given two reasonable sets of estimates for the a priori spatiotemporal error correlation lengths.

4.3 Other sources of error

This analysis did not evaluate the impact of potential systematic errors (biases) in the observations or the transport model, which are not well represented by the Gaussian errors assumed in traditional linear error analysis (Baker et al., 2010). Chevallier et al. (2007) demonstrated that potential biases in OCO satellite CO₂ measurements related to the presence of aerosols can completely negate the improvements to prior uncertainties provided by the measurements for the most polluted land regions and for ocean regions. In another OCO OSSE, Baker et al. (2010) found that a combination of systematic errors from aerosols, model transport, and incorrectly-assumed statistics could degrade both the magni-

tude and spatial extent of uncertainty improvements by about a factor of two over land and even more over the ocean. Thus, it will be important to control systematic errors in ASCENDS observations and the transport model as well as minimizing random errors. Note that systematic observation errors can be expected to decrease over the course of the mission as adjustments are made to the measurement system and to the retrieval algorithms in calibration/validation activities.

4.4 Other considerations in evaluating ASCENDS

The potential combined use of multiple wavelengths in the ASCENDS measurements, e.g., various offsets from 1.57 μm , could provide additional information on surface fluxes given the sensitivities to concentrations at different levels of the atmosphere. Furthermore, other CO₂ data sets will certainly be available alongside ASCENDS data (e.g., from in situ networks), and the combination of data sets will provide stronger constraints on fluxes than any individual data set (Hungershoefer et al., 2010).

Our comparison of the results for the 1.57 and 2.05 μm wavelengths over North America may be less applicable to other parts of the world. The global OSSE study by Hungershoefer et al. (2010), which compared various observing systems including a satellite lidar system similar to ASCENDS, A-SCOPE, found that the 1.6 μm wavelength results in larger uncertainty reductions over South America but performs less well than 2.0 μm over temperate and cold regions. They attribute the better performance of 1.6 μm over South America to the strong vertical mixing of air there, which lessens the disadvantage of that wavelength's having weaker sensitivity to the lower troposphere. However, they used a simpler error formulation. On the other hand, in our global inversion, 2.05 μm results in 8 % larger uncertainty reductions than 1.57 μm throughout the world on average (for RRV error of 0.5–1.0 ppm).

5 Conclusions

We have conducted an observing system simulation for North America using projected ASCENDS observation uncertainty estimates and a novel approach utilizing a portable footprint library generated from a high-resolution Lagrangian transport model to quantify the surface CO₂ flux constraints provided by the future observations. We consider four possible configurations for the active optical remote sensing instrument covering two weighting functions and two random error levels. We find that the ASCENDS observations potentially reduce flux uncertainties substantially at fine and biome scales. At the $1^\circ \times 1^\circ$ grid scale, weekly uncertainty reductions up to 30–45 % (averaged over the year) are achieved depending on the presumed instrument configuration. Relatively large uncertainty reductions occur year-round in southern Mexico and the Pacific Northwest and seasonally in the

southeastern and mid-western U.S. and parts of Canada and Alaska, when and where there is good coverage by observations with low uncertainties and a priori uncertainties are large. Uncertainty reductions at the annual biome scale range from $\sim 40\%$ to $\sim 75\%$ across the four experimental cases, and from $\sim 65\%$ to $\sim 85\%$ for the continent as a whole. The uncertainty reductions for the 1.57 μm candidate wavelength are on average 10 % smaller than those for 2.05 μm across the biomes and the two RRV reference error levels; for 0.5 ppm RRV error the uncertainty reductions are on average $\sim 25\%$ larger than those for 1.0 ppm error across biomes and the two wavelengths.

Based on the flux precision on an annual biome scale suggested by Hungershoefer et al. (2010) for understanding the global carbon sink and feedbacks, ASCENDS observations would meet a threshold requirement for all biomes within the range of the measurement designs considered here. The observations constrain a posteriori uncertainties to a level of 0.01–0.06 Pg C yr⁻¹ and could thus help pin down the location and magnitude of long-term C sinks. With regards to the more stringent target requirement, a subset of the instrument designs would meet the target for a majority of biomes.

The results we have presented may be optimistic, since potential systematic errors in the observations, boundary conditions, and transport model that we have neglected would degrade the flux estimates. However, modifications to the size and location of our regional domain (e.g., an eastward shift) could improve the constraints by satellite observations on North American fluxes. In addition, our consideration of different measures of the impact of observations on flux estimates, such as posterior uncertainty and uncertainty reduction, strengthens the study, given that different measures can be affected differently by assumptions such as prior uncertainties.

In future work, inversions in various regions (including, for example, South America) with a more comprehensive treatment of error sources could more definitively establish the usefulness of ASCENDS observations for constraining fluxes at fine and large scales and answering global carbon cycle science questions.

Acknowledgements. Work at NASA and AER has been supported by the NASA Atmospheric CO₂ Observations from Space program element and NASA ASCENDS pre-phase A activity funding. We are grateful to the NASA Ames HEC facility staff for assistance in executing the WRF–STILT runs on the Pleiades supercomputer, and to the NASA HEC Program for granting use of the Dali and Discover systems at the NASA Center for Climate Simulation. We also thank J. Abshire, E. Browell, and R. Menzies for contributions to ASCENDS data characterization, G. J. Collatz for making available the CASA–GFED fluxes that we used to construct the a priori uncertainties, R. Aschbrenner for help with the footprint calculations, S. Gourdji for providing correlation parameters and the biome map, P. Rayner and A. Michalak for advice on inversions, M. Manyin and Y. Liu for computing help, L. Ott for

help with transferring WRF–STILT files, and G. J. Collatz and E. McGrath-Spangler for comments on the manuscript. Finally, we appreciate the comments provided by two anonymous referees.

Edited by: M. Kopacz

References

- Baker, D. F., Bösch, H., Doney, S. C., O'Brien, D., and Schimel, D. S.: Carbon source/sink information provided by column CO₂ measurements from the Orbiting Carbon Observatory, *Atmos. Chem. Phys.*, 10, 4145–4165, doi:10.5194/acp-10-4145-2010, 2010.
- Basu, S., Guerlet, S., Butz, A., Houweling, S., Hasekamp, O., Aben, I., Krummel, P., Steele, P., Langenfelds, R., Torn, M., Biraud, S., Stephens, B., Andrews, A., and Worthy, D.: Global CO₂ fluxes estimated from GOSAT retrievals of total column CO₂, *Atmos. Chem. Phys.*, 13, 8695–8717, doi:10.5194/acp-13-8695-2013, 2013.
- Bocquet, M., Wu, L., and Chevallier, F.: Bayesian design of control space for optimal assimilation of observations. Part I: Consistent multiscale formalism, *Q. J. R. Meteorol. Soc.*, 137, 1340–1356, doi:10.1002/qj.837, 2011.
- Brioude, J., Kim, S.-W., Angevine, W. M., Frost, G. J., Lee, S.-H., McKeen, S. A., Trainer, M., Fehsenfeld, F. C., Holloway, J. S., Ryerson, T. B., Williams, E. J., Petron, G., and Fast, J. D.: Top-down estimate of anthropogenic emission inventories and interannual variability in Houston using a mesoscale inverse modeling technique, *J. Geophys. Res.*, 116, D20305, doi:10.1029/2011JD016215, 2011.
- Brioude, J., Petron, G., Frost, G. J., Ahmadov, R., Angevine, W. M., Hsie, E.-Y., Kim, S.-W., Lee, S.-H., McKeen, S. A., Trainer, M., Fehsenfeld, F. C., Holloway, J. S., Peischl, J., Ryerson, T. B., and Gurney, K. R.: A new inversion method to calculate emission inventories without a prior at mesoscale: Application to the anthropogenic CO₂ emission from Houston, Texas, *J. Geophys. Res.*, 117, D05312, doi:10.1029/2011JD016918, 2012.
- Brioude, J., Angevine, W. M., Ahmadov, R., Kim, S.-W., Evan, S., McKeen, S. A., Hsie, E.-Y., Frost, G. J., Neuman, J. A., Pollack, I. B., Peischl, J., Ryerson, T. B., Holloway, J., Brown, S. S., Nowak, J. B., Roberts, J. M., Wofsy, S. C., Santoni, G. W., Oda, T., and Trainer, M.: Top-down estimate of surface flux in the Los Angeles Basin using a mesoscale inverse modeling technique: assessing anthropogenic emissions of CO, NO_x and CO₂ and their impacts, *Atmos. Chem. Phys.*, 13, 3661–3677, doi:10.5194/acp-13-3661-2013, 2013.
- Butler, M. P., Davis, K. J., Denning, A. S., and Kawa, S. R.: Using continental observations in global atmospheric inversions of CO₂: North American carbon sources and sinks, *Tellus*, 62B, 550–572, doi:10.1111/j.1600-0889.2010.00501.x, 2010.
- Caron, J., and Durand, Y.: Operating wavelengths optimization for a spaceborne lidar measuring atmospheric CO₂, *Appl. Opt.*, 48, 5413–5422, 2009.
- Chevallier, F., Bréon, F.-M., and Rayner, P. J.: Contribution of the Orbiting Carbon Observatory to the estimation of CO₂ sources and sinks: Theoretical study in a variational data assimilation framework, *J. Geophys. Res.*, 112, D09307, doi:10.1029/2006JD007375, 2007.
- Crisp, D., Miller, C. E., and DeCola, P. L.: NASA Orbiting Carbon Observatory: measuring the column averaged carbon dioxide mole fraction from space, *J. Appl. Remote Sens.*, 2, 023508, doi:10.1117/1.2898457, 2008.
- Deng, F., Jones, D. B. A., Henze, D. K., Bousserez, N., Bowman, K. W., Fisher, J. B., Nassar, R., O'Dell, C., Wunch, D., Wennberg, P. O., Kort, E. A., Wofsy, S. C., Blumenstock, T., Deutscher, N. M., Griffith, D. W. T., Hase, F., Heikkinen, P., Sherlock, V., Strong, K., Sussmann, R., and Warneke, T.: Inferring regional sources and sinks of atmospheric CO₂ from GOSAT XCO₂ data, *Atmos. Chem. Phys.*, 14, 3703–3727, doi:10.5194/acp-14-3703-2014, 2014.
- Dlugokencky, E. J., Lang, P. M., Masarie, K. A., Crotwell, A. M., and Crotwell, M. J.: Atmospheric Carbon Dioxide Dry Air Mole Fractions from the NOAA ESRL Carbon Cycle Cooperative Global Air Sampling Network, 1968–2012, Version: 2013-08-28, available at: ftp://aftp.cmdl.noaa.gov/data/trace_gases/co2/flask/surface/ (last access: 18 February 2014), 2013.
- Eldering, A., Solish, B., Kahn, P., Boland, S., Crisp, D., and Gunson, M.: High precision atmospheric CO₂ measurements from space: the design and implementation of OCO-2, *IEEE Aerospace Conference Proceedings*, 1805–1814, 2012.
- Engelen, R. J., Denning, A. S., and Gurney, K. R.: On error estimation in atmospheric CO₂ inversions, *J. Geophys. Res.*, 107, 4635, doi:10.1029/2002JD002195, 2002.
- Enting, I. G., Trudinger, C. M., and Francey, R. J.: A synthesis inversion of the concentration and δ¹³C of atmospheric CO₂, *Tellus*, 47B, 35–52, 1995.
- Feng, L., Palmer, P. I., Boesch, H., and Dance, S.: Estimating surface CO₂ fluxes from space-borne CO₂ dry air mole fraction observations using an ensemble Kalman Filter, *Atmos. Chem. Phys.*, 9, 2619–2633, doi:10.5194/acp-9-2619-2009, 2009.
- Gerbig, C., Lin, J. C., Wofsy, S. C., Daube, B. C., Andrews, A. E., Stephens, B. B., Bakwin, P. S., and Grainger, C. A.: Towards constraining regional scale fluxes of CO₂ with atmospheric observations over a continent: 2. Analysis of COBRA data using a receptor-oriented framework, *J. Geophys. Res.*, 108, 4757, doi:10.1029/2003JD003770, 2003.
- Göckede, M., Michalak, A. M., Vickers, D., Turner, D. P., and Law, B. E.: Atmospheric inverse modeling to constrain regional scale CO₂ budgets at high spatial and temporal resolution, *J. Geophys. Res.*, 115, D15113, doi:10.1029/2009JD012257, 2010a.
- Göckede, M., Turner, D. P., Michalak, A. M., Vickers, D., and Law, B. E.: Sensitivity of a subregional scale atmospheric inverse CO₂ modeling framework to boundary conditions, *J. Geophys. Res.*, 115, D24112, doi:10.1029/2010JD014443, 2010b.
- Gourdji, S. M., Mueller, K. L., Yadav, V., Huntzinger, D. N., Andrews, A. E., Trudeau, M., Petron, G., Nehr Korn, T., Eluszkiewicz, J., Henderson, J., Wen, D., Lin, J., Fischer, M., Sweeney, C., and Michalak, A. M.: North American CO₂ exchange: inter-comparison of modeled estimates with results from a fine-scale atmospheric inversion, *Biogeosciences*, 9, 457–475, doi:10.5194/bg-9-457-2012, 2012.
- Gurney, K. R., Mendoza, D. L., Zhou, Y., Fischer, M. L., Miller, C. C., Geethakumar, S., and de la Rue du Can, S.: High resolution fossil fuel combustion CO₂ emission fluxes for the United States, *Environ. Sci. Technol.*, 43, 5535–5541, doi:10.1021/es900806c, 2009.

- Houweling, S., Breon, F.-M., Aben, I., Rödenbeck, C., Gloor, M., Heimann, M., and Ciais, P.: Inverse modeling of CO₂ sources and sinks using satellite data: a synthetic inter-comparison of measurement techniques and their performance as a function of space and time, *Atmos. Chem. Phys.*, 4, 523–538, doi:10.5194/acp-4-523-2004, 2004.
- Hungerschofer, K., Breon, F.-M., Peylin, P., Chevallier, F., Rayner, P., Klonecki, A., Houweling, S., and Marshall, J.: Evaluation of various observing systems for the global monitoring of CO₂ surface fluxes, *Atmos. Chem. Phys.*, 10, 10503–10520, doi:10.5194/acp-10-10503-2010, 2010.
- Huntzinger, D. N., Post, W. M., Wei, Y., Michalak, A. M., West, T. O., Jacobson, A. R., Baker, I. T., Chen, J. M., Davis, K. J., Hayes, D. J., Hoffman, F. M., Jain, A. K., Liu, S., McGuire, A. D., Neilson, R. P., Potter, C., Poulter, B., Price, D., Raczka, B. M., Tian, H. Q., Thornton, P., Tomelleri, E., Viovy, N., Xiao, J., Yuan, W., Zeng, N., Zhao, M., and Cook, R.: North American Carbon Program (NACP) regional interim synthesis: terrestrial biospheric model intercomparison, *Ecol. Model.*, 232, 144–157, doi:10.1016/j.ecolmodel.2012.02.004, 2012.
- Hu, Y., Stamnes, K., Vaughan, M., Pelon, J., Weimer, C., Wu, D., Cisewski, M., Sun, W., Yang, P., Lin, B., Omar, A., Flittner, D., Hostetler, C., Trepte, C., Winker, D., Gibson, G., and Santa-Maria, M.: Sea surface wind speed estimation from space-based lidar measurements, *Atmos. Chem. Phys.*, 8, 3593–3601, doi:10.5194/acp-8-3593-2008, 2008.
- Ingmann, P.: A-SCOPE, Advanced Space Carbon and Climate Observation of Planet Earth, Report for Assessment, SP-1313/1, ESA Communication Production Office, Noordwijk, the Netherlands, 2008.
- Kaminski, T., Rayner, P., Heimann, M., and Enting, I.: On aggregation errors in atmospheric transport inversions, *J. Geophys. Res.*, 106, 4703–4715, 2001.
- Kaminski, T., Scholze, M., and Houweling, S.: Quantifying the benefit of A-SCOPE data for reducing uncertainties in terrestrial carbon fluxes in CCDAS, *Tellus*, 62B, 784–796, 2010.
- Kawa, S. R., Erickson III, D. J., Pawson, S., and Zhu, Z.: Global CO₂ transport simulations using meteorological data from the NASA data assimilation system, *J. Geophys. Res.*, 109, D18312, doi:10.1029/2004JD004554, 2004.
- Kawa, S. R., Mao, J., Abshire, J. B., Collatz, G. J., Sun, X., and Weaver, C. J.: Simulation studies for a space-based CO₂ lidar mission, *Tellus B*, 62, 759–769, doi:10.1111/j.1600-0889.2010.00486.x, 2010.
- Kort, E. A., Eluszkiewicz, J., Stephens, B. B., Miller, J. B., Gerbig, C., Nehrkorn, T., Daube, B. C., Kaplan, J. O., Houweling, S., and Wofsy, S. C.: Emissions of CH₄ and N₂O over the United States and Canada based on a receptor-oriented modeling framework and COBRA-NA atmospheric observations, *Geophys. Res. Lett.*, 35, L18808, doi:10.1029/2008GL034031, 2008.
- Kort, E. A., Andrews, A. E., Dlugokencky, E., Sweeney, C., Hirsch, A., Eluszkiewicz, J., Nehrkorn, T., Michalak, A., Stephens, B., Gerbig, C., Miller, J. B., Kaplan, J., Houweling, S., Daube, B. C., Tans, P., and Wofsy, S. C.: Atmospheric constraints on 2004 emissions of methane and nitrous oxide in North America from atmospheric measurements and receptor-oriented modeling framework, *J. Integr. Environ. Sci.*, 7, 125–133, 2010.
- Lauvaux, T., Schuh, A. E., Uliasz, M., Richardson, S., Miles, N., Andrews, A. E., Sweeney, C., Diaz, L. I., Martins, D., Shepson, P. B., and Davis, K. J.: Constraining the CO₂ budget of the corn belt: exploring uncertainties from the assumptions in a mesoscale inverse system, *Atmos. Chem. Phys.*, 12, 337–354, doi:10.5194/acp-12-337-2012, 2012.
- Le Quéré, C., Andres, R. J., Boden, T., Conway, T., Houghton, R. A., House, J. I., Marland, G., Peters, G. P., van der Werf, G., Ahlström, A., Andrew, R. M., Bopp, L., Canadell, J. G., Ciais, P., Doney, S. C., Enright, C., Friedlingstein, P., Huntingford, C., Jain, A. K., Jourdain, C., Kato, E., Keeling, R. F., Klein Goldewijk, K., Levis, S., Levy, P., Lomas, M., Poulter, B., Raupach, M. R., Schwinger, J., Sitch, S., Stocker, B. D., Viovy, N., Zaehle, S., and Zeng, N.: The global carbon budget 1959–2011, *Earth Syst. Sci. Data Discuss.*, 5, 1107–1157, doi:10.5194/essdd-5-1107-2012, 2012.
- Lin, J. C., Gerbig, C., Wofsy, S. C., Daube, B. C., Andrews, A. E., Davis, K. J., and Grainger, C. A.: A near-field tool for simulating the upstream influence of atmospheric observations: the Stochastic Time-Inverted Lagrangian Transport (STILT) model, *J. Geophys. Res.*, 108, 4493, doi:10.1029/2002JD003161, 2003.
- McKain, K., Wofsy, S. C., Nehrkorn, T., Eluszkiewicz, J., Ehleringer, J. R., and Stephens, B. B.: Assessment of ground-based atmospheric observations for verification of greenhouse gas emissions from an urban region, *Proc. Natl. Acad. Sci. USA*, 109, 8423–8428, 2012.
- Miller, S. M., Kort, E. A., Hirsch, A. I., Dlugokencky, E. J., Andrews, A. E., Xu, X., Tian, H., Nehrkorn, T., Eluszkiewicz, J., Michalak, A. M., and Wofsy, S. C.: Regional sources of nitrous oxide over the United States: seasonal variation and spatial distribution, *J. Geophys. Res.*, 117, D06310, doi:10.1029/2011JD016951, 2012.
- Miller, S. M., Wofsy, S. C., Michalak, A. M., Kort, E. A., Andrews, A. E., Biraud, S. C., Dlugokencky, E. J., Eluszkiewicz, J., Fischer, M. L., Janssens-Maenhout, G., Miller, B. R., Miller, J. B., Montzka, S. A., Nehrkorn, T., and Sweeney, C.: Anthropogenic emissions of methane in the United States, *Proc. Natl. Acad. Sci. USA*, 110, 20018–20022, doi:10.1073/pnas.1314392110, 2013.
- National Research Council: Earth Science and Applications from Space: National Imperatives for the Next Decade and Beyond, The National Academies Press, Washington, DC, 2007.
- Nehrkorn, T., Eluszkiewicz, J., Wofsy, S. C., Lin, J. C., Gerbig, C., Longo, M., and Freitas, S.: Coupled Weather Research and Forecasting/Stochastic Time-Inverted Lagrangian Transport (WRF-STILT) model, *Meteor. Atmos. Phys.*, 107, 51–64, doi:10.1007/s00703-010-0068-x, 2010.
- Olson, D. M., Dinerstein, E., Wikramanayake, E. D., Burgess, N. D., Powell, G. V. N., Underwood, E. C., D'Amico, J. A., Itoua, I., Strand, H. E., Morrison, J. C., Loucks, C. J., Allnutt, T. F., Ricketts, T. H., Kura, Y., Lamoreux, J. F., Wettengel, W. W., Hedao, P., and Kassem, K. R.: Terrestrial ecoregions of the world: a new map of life on earth, *Bioscience*, 51, 933–938, 2001.
- Peters, W., Jacobson, A. R., Sweeney, C., Andrews, A. E., Conway, T. J., Masarie, K., Miller, J. B., Bruhwiler, L. M. P., Petron, G., Hirsch, A. I., Worthy, D. E. J., van der Werf, G. R., Randerson, J. T., Wennberg, P. O., Krol, M. C., and Tans, P. P.: An atmospheric perspective on North American carbon dioxide exchange: Carbon Tracker, *P. Natl. Acad. Sci. USA*, 104, 18925–18930, 2007.
- Pillai, D., Gerbig, C., Marshall, J., Ahmadov, R., Kretschmer, R., Koch, T., and Karstens, U.: High resolution modeling of CO₂ over Europe: implications for representation errors of satellite

- retrievals, *Atmos. Chem. Phys.*, 10, 83–94, doi:10.5194/acp-10-83-2010, 2010.
- Randerson, J. T., Thompson, M. V., and Malmstrom, C. M.: Substrate limitations for heterotrophs: implications for models that estimate the seasonal cycle of atmospheric CO₂, *Global Biogeochem. Cycles*, 10, 585–602, 1996.
- Rayner, P. J., Enting, I. G., Francey, R. J. and Langenfelds, R.: Reconstructing the recent carbon cycle from atmospheric CO₂, δ¹³C and O₂/N₂ observations, *Tellus B*, 51, 213–232, 1999.
- Rayner, P. J., and O'Brien, D. M.: The utility of remotely sensed CO₂ concentration data in surface source inversions, *Geophys. Res. Lett.*, 28, 175–178, 2001.
- Rienecker, M. M., Suarez, M. J., Gelaro, R., Todling, R., Bacmeister, J., Liu, E., Bosilovich, M. G., Schubert, S. D., Takacs, L., Kim, G.-K., Bloom, S., Chen, J., Collins, D., Conaty, A., Da Silva, A., Gu, W., Joiner, J., Koster, R. D., Lucchesi, R., Molod, A., Owens, T., Pawson, S., Pegion, P., Redder, C. R., Reichle, R., Robertson, F. R., Ruddick, A. G., Sienkiewicz, M., and Woollen, J.: MERRA: NASA's Modern-Era Retrospective Analysis for Research and Applications, *J. Climate*, 24, 3624–3648, 2011.
- Rodgers, C. D.: *Inverse Methods for Atmospheric Sounding: Theory and Practice*, World Scientific, Singapore, 2000.
- Schuh, A. E., Denning, A. S., Corbin, K. D., Baker, I. T., Uliasz, M., Parazoo, N., Andrews, A. E., and Worthy, D. E. J.: A regional high-resolution carbon flux inversion of North America for 2004, *Biogeosciences*, 7, 1625–1644, doi:10.5194/bg-7-1625-2010, 2010.
- Skamarock, W. C., and Klemp, J. B.: A time-split nonhydrostatic atmospheric model for weather research and forecasting applications, *J. Comp. Phys.*, 227, 3465–3485, 2008.
- van der Werf, G. R., Randerson, J. T., Giglio, L., Collatz, G. J., Kasibhatla, P. S., and Arellano Jr., A. F.: Interannual variability in global biomass burning emissions from 1997 to 2004, *Atmos. Chem. Phys.*, 6, 3423–3441, doi:10.5194/acp-6-3423-2006, 2006.
- van der Werf, G. R., Randerson, J. T., Giglio, L., Collatz, G. J., Mu, M., Kasibhatla, P. S., Morton, D. C., DeFries, R. S., Jin, Y., and van Leeuwen, T. T.: Global fire emissions and the contribution of deforestation, savanna, forest, agricultural, and peat fires (1997–2009), *Atmos. Chem. Phys.*, 10, 11707–11735, doi:10.5194/acp-10-11707-2010, 2010.
- Wang, J. S., McElroy, M. B., Logan, J. A., Palmer, P. I., Chameides, W. L., Wang, Y., and Megretskaya, I. A.: A quantitative assessment of uncertainties affecting estimates of global mean OH derived from methyl chloroform observations, *J. Geophys. Res.*, 113, D12302, doi:10.1029/2007JD008496, 2008.
- Yokota, T., Yoshida, Y., Eguchi, N., Ota, Y., Tanaka, T., Watanabe, H., and Maksyutov, S.: Global concentrations of CO₂ and CH₄ retrieved from GOSAT: first preliminary results, *SOLA*, 5, 160–163, doi:10.2151/sola.2009-041, 2009.
- Zhao, C., Andrews, A. E., Bianco, L., Eluszkiewicz, J., Hirsch, A., MacDonald, C., Nehr Korn, T., and Fischer, M. L.: Atmospheric inverse estimates of methane emissions from Central California, *J. Geophys. Res.*, 114, D16302, doi:10.1029/2008JD011671, 2009.